Phase-coherent control of the molecular polar order in polymers using dual-frequency interferences between circularly polarized beams

Anne-Catherine Etilé, Céline Fiorini,* Fabrice Charra, and Jean-Michel Nunzi
LETI (CEA-Technologies Avancées), CEA Saclay, DEIN-SPE, Groupe Composants Organiques, 91191 Gif-sur-Yvette Cedex, France
(Received 5 May 1997)

Dual-frequency interferences using appropriate combinations of circular writing beam polarizations are demonstrated to enable full control of the molecular polar order in a polymer. A comparative theoretical and experimental analysis of the all-optical poling process in the cases of linear, cohelical, and counterhelical writing polarizations is achieved. Dynamics, efficiency, phase matching, and tensorial aspects are analyzed. Nearly perfect dipolar and octupolar ordering is achieved using conventional one-dimensional molecules. As a feature of dual-frequency holography with circular polarizations, writing beam phase retardation $\Delta\Phi$ is coded into a $\chi^{(2)}$ pattern rotation by the same angle. Interestingly, in the case of a fundamental beam with linear polarization, second harmonic generation is independent of the polarization direction.
[S1050-2947(97)06010-1]

PACS number(s): 33.80.Be

I. INTRODUCTION

From holographic storage to optical trapping or molecular addressing, optical manipulation is a field of growing interest. Indeed the great latitude and flexibility of optical means offers interesting prospects. One challenging issue is to make use not only of the high power or spectral selectivity of laser beams but also to take full advantage of the coherence properties of lasers. In this respect, it is necessary to generalize the principles of holography to the recording of an interference pattern between mutually coherent fields of different frequencies. Interestingly, through nonlinear light-matter interaction, multiple frequency mixing can induce directional effects such as polar order.

Efficient coherent radiative control of chemical reactions such as photodissociation or control of photocurrent generation in semiconductors was recently demonstrated using quantum interferences between multiphoton absorption processes [1,2]. Dual-frequency phase-coherent laser excitation at fundamental and second harmonic (SH) frequencies was also shown to lead to efficient $\chi^{(2)}$ encoding in silica-based glasses [3–7] and more recently in organics [8,9].

In the case of organics, the physical origin of photoinduced centrosymmetry breaking was identified as a selective excitation of the molecules oriented in one given direction and sense via simultaneous one- and two-photon absorption on the same electronic level. Optimization of the relative phase and energy between the writing beams at frequencies ω and 2ω permitted the achievement of large orientation efficiency in azo-dye copolymers [10].

One breakthrough with such an all-optical poling technique is that it leads to an automatic molecular organization with a period satisfying the phase-matching conditions for second harmonic generation. Additionally, using molecules with specific geometries, such as the octupolar molecules, it was recently shown that the coherent superposition of two linearly polarized writing fields E_ω and $E_{2\omega}$ also results in specific symmetries of the macroscopic polar order [11,12].

In this paper, we show that using appropriate combinations of adequately polarized writing beams at fundamental and SH frequencies, it is possible to tailor the symmetry resulting from nonlinear absorption of the dual-frequency poling field $E(t)=E_\omega(t)+E_{2\omega}(t)$, even using one-dimensional molecules. This enables a complete in-plane engineering of the photoinduced polar order. The tensor properties of the photoinduced second-order susceptibility $\chi^{(2)}$ are analyzed. We show that in the case of helical writing beams, an angular encoding of the phase difference of the cubic interference process is achieved. This leads to a polarization-independent second harmonic generation in the case of a fundamental linear polarization. Dynamics, efficiency, and symmetry implications of the writing-beam polarization-dependent photoinduced polar order are discussed. Consequences on the $\chi^{(2)}$ phase-matching efficiency are reported.

II. PHOTOINDUCED ORIENTATION PROCESS: INFLUENCE OF THE WRITING BEAM POLARIZATIONS

A. Selective polar photoexcitation

As suggested by Baranova and Zel'dovich [13], the interference between a light wave and its second harmonic prints a photoinduced $\chi^{(2)}$ resulting from a selective polar excitation of the individual molecules [14]. Indeed, a molecule excited in resonance with the fields E_ω and $E_{2\omega}$ at fundamental and second harmonic frequencies experiences simultaneous one- and two-photon absorptions on the same electronic transition $0\rightarrow 1$.

The average energy absorbed by a molecule in the field $\mathbf{E}(t)=\mathbf{E}_{2\omega}(t)+\mathbf{E}_\omega(t)$ contains a polar contribution ρ_{01} that results in a breaking of the initial centrosymmetry of the material, leaving a new distribution of molecules $N_P(M)$ exhibiting polar order [15]:

$$N_P(M)\propto\rho_{01}(M)\propto\overline{\overline{\beta}}''\cdot(\mathbf{E}_{2\omega}^{*}\otimes\mathbf{E}_\omega\otimes\mathbf{E}_\omega)+\text{c.c.}, \qquad (1)$$

*Author to whom correspondence should be addressed. FAX: (+33) 01 69 08 76 79. Electronic address: fiorini@serin.cea.fr

where $\overline{\overline{\overline{\beta}}}$ is the imaginary part of the molecular hyperpolarizability tensor $\overline{\overline{\overline{\beta}}}$ (β stands for its norm). The center dot represents tensorial contraction, i.e., summation between repeated indices.

In the case of one-dimensional molecules, the hyperpolarizability tensor writes $\overline{\overline{\overline{\beta}}}=\beta(\mathbf{x}\otimes\mathbf{x}\otimes\mathbf{x})$, with $\mathbf{x}$ the molecular axis, so that the polar distribution of molecules $N_P(M)$ becomes

$$N_P(M)\propto(\mathbf{E}_{2\omega}^{*}\cdot\mathbf{x})(\mathbf{E}_{\omega}\cdot\mathbf{x})(\mathbf{E}_{\omega}\cdot\mathbf{x})+\text{c.c.}, \tag{2}$$

where $\mathbf{E}_{\omega}=\widetilde{E}_{\omega}\exp(-ik_{\omega}z)\boldsymbol{\varepsilon}_{\omega}$ and $\mathbf{E}_{2\omega}=\widetilde{E}_{2\omega}\exp-i(k_{2\omega}z+\Delta\Phi)\boldsymbol{\varepsilon}_{2\omega}$, with $\mathbf{k}_{\omega}$ and $\mathbf{k}_{2\omega}$, the wave vectors at frequencies ω and 2ω. $\Delta\Phi$ is the phase difference between writing beams at frequencies ω and 2ω. $\widetilde{E}_{\omega}$ and $\widetilde{E}_{2\omega}$ are the writing fields amplitudes at frequencies ω and 2ω, respectively. $\boldsymbol{\varepsilon}_{\omega}$ and $\boldsymbol{\varepsilon}_{2\omega}$ are the polarization states of the beams at frequencies ω and 2ω.

In the particular case of linear and circular polarizations of the writing beams at ω and 2ω frequencies: $\boldsymbol{\varepsilon}_{\omega}=(1/\sqrt{1+\varepsilon_1^2})(\mathbf{X}+i\varepsilon_1\mathbf{Y})$ and $\boldsymbol{\varepsilon}_{2\omega}=(1/\sqrt{1+\varepsilon_2^2})(\mathbf{X}+i\varepsilon_2\mathbf{Y})$, with $\varepsilon_1=\varepsilon_2=0$ for linear polarizations and $\varepsilon_1=\varepsilon_2=1$ or $\varepsilon_1=-\varepsilon_2=1$ for cohelical or counterhelical polarizations, respectively. $1/\sqrt{1+\varepsilon_1^2}$ and $1/\sqrt{1+\varepsilon_2^2}$ are normalization factors. Representation of the molecular axis in a reference set of axes (X,Y,Z) is shown in Fig. 1. Polar coordinates are referenced by the Euler angles (θ,φ). Developing Eq. (2), the photoinduced polar distribution $N_p(M)$ becomes

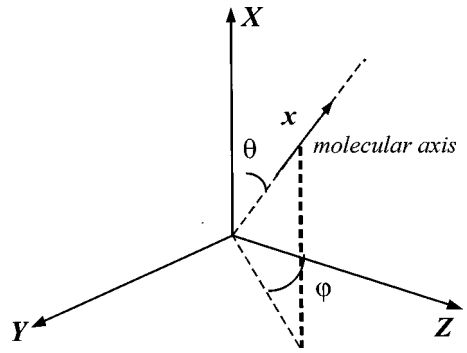

FIG. 1. Representation of the molecular axis x in a reference set of axes (X,Y,Z). The polar molecular coordinates are the Euler angles (θ,φ).

$$N_P(M)\propto\frac{1}{(1+\varepsilon_1^2)\sqrt{(1+\varepsilon_2^2)}}[\cos(\Delta k\cdot z+\Delta\Phi)(\cos^3\theta+(2\varepsilon_1\varepsilon_2-\varepsilon_1^2)\cos\theta\,\sin^2\theta\,\sin^2\varphi)-\sin(\Delta k\cdot z+\Delta\Phi)$$
$$\times(\varepsilon_1^2\varepsilon_2\sin^3\theta\,\sin^3\varphi+(2\varepsilon_1-\varepsilon_2)\cos^2\theta\,\sin\theta\,\sin\varphi], \tag{3}$$

with $\Delta k=2k_{\omega}-k_{2\omega}$, the wave-vector mismatch.

We show in the following that symmetry of the photoinduced polar distribution $N_P(M)$ is strongly dependent on the polarization combinations of the writing beams. This determines the photoinduced molecular polar orientation process.

B. Analysis of the photoinduced polar order

Full characterization of the photoinduced polar order is deduced from the tensor analysis of the photoinduced second-order susceptibility $\chi^{(2)}$. In the case of an assembly of noninteracting molecules, the macroscopic second-order susceptibility $\chi^{(2)}$ is determined by microscopic light-molecule interaction. Averaging microscopic interactions over all orientations [16], we get

$$\chi_{\Delta\Delta\Delta}^{(2)}=\eta\int N_P\beta_{\Delta\Delta\Delta}(\Omega)d\Omega/\varepsilon_0, \tag{4}$$

where Δ is a given direction in the (X,Y) plane of the sample. η stands for the efficiency of the molecular reorientation process following selective polar excitation. $\beta_{\Delta\Delta\Delta}$ is the projection of the molecular hyperpolarizability $\overline{\overline{\overline{\beta}}}$ on Δ: $\beta_{\Delta\Delta\Delta}(\Omega)=\Sigma_{x,y,z}(\Delta\cdot x)(\Delta\cdot y)(\Delta\cdot z)\beta_{xyz}$, x,y,z standing for unit vectors in the molecular frame. Projection factors depend on Euler angles θ, φ in Fig. 1. $d\Omega$ is the normalized element of solid angle. Local field factors are not explicitly mentioned and may be considered as implicitly included into β.

Details of the calculation for different writing beam polarizations are developed in the Appendix. Incidence of the writing beam polarizations on $\chi^{(2)}$ is discussed in the following section in view of both experimental results and theoretical predictions.

III. RESULTS AND DISCUSSION

A. Seeding-type experiment

As already described, the experiment consists in a seeding-type setup [9]. The source was a Nd:YAG laser delivering 25-ps pulses at 1064 nm with a 10-Hz repetition rate. Writing and probing periods were alternated. Writing periods correspond to the simultaneous irradiation of the sample by the coherent superposition of the 1064-nm fundamental and the 532-nm second harmonic. Second harmonics is obtained by frequency doubling of the fundamental beam in a potassium dihydride phosphate (KDP) crystal.

Fundamental and second harmonic writing beam fluences were optimized in order to reach the maximum poling efficiency. Indeed, as expected for an interference process, all-optical poling efficiency depends on the relative intensities of the writing beams. More precisely, optimization of the cubic interference fringe contrast requires equal one- and two-photon excitation probabilities [10]. During the writing process, the relative phase $\Delta\Phi$ between writing beams at ω and 2ω frequencies was adjusted by tilting a BK7 plate with

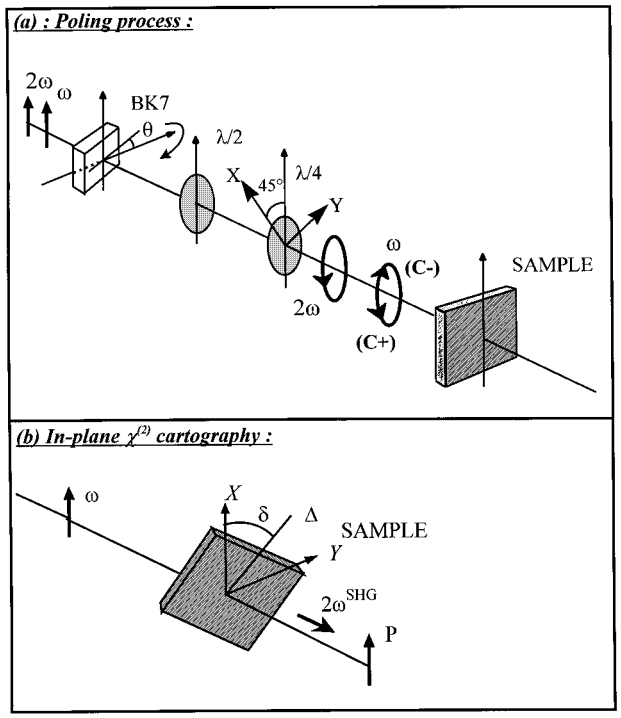

FIG. 2. Schematic representation of the seeding-type experimental setup. The upper part (a) shows the writing process. During the writing process, the relative phase $\Delta\Phi$ between writing beams at ω and 2ω frequencies is adjusted by tilting a BK7 plate with known thickness and index dispersion. Indeed, in the limit of small writing beams incidence angle θ, $\Delta\Phi=\pi\Delta n_{\mathrm{BK7}}t_{\mathrm{BK7}}\theta^2/n^2\lambda_{2\omega}$, with $\Delta n_{\mathrm{BK7}}=n_{2\omega}-n_{\omega}$ and t_{BK7}, the BK7 dispersion and thickness, respectively. Polarizations at ω and 2ω are varied using bichromatic half- and quarter-wave plates. In both cases of cohelicities $(C+)$ or counterhelicities $(C-)$ of the writing beams, power measurements gave eccentricities e defined as $e=(P_{\max}-P_{\min})/(P_{\max}+P_{\min})$ smaller than 5%. The lower part (b) shows the setup for polar in-plane analysis of the photoinduced $\chi^{(2)}$. For this purpose a linearly polarized reading beam at fundamental frequency is used and the SH signal is analyzed along the same direction. A green blocking RG630-Schott filter is used to leave only the fundamental beam incident on the sample. The sample is mounted on a rotating stage enabling in-plane rotation. The reference set of axes X,Y corresponds to the neutral axes of the quarter-wave plate.

known thickness and index dispersion [Fig. 2(a)].

Three different polarization combinations for the writing beams at frequencies ω and 2ω have been studied and compared: linear polarizations, cohelical polarizations, and counterhelical polarizations. In the first case, the two writing beams were simply polarized using a Glan polarizer. In order to get collinear copropagating circularly polarized ω and 2ω writing beams, a bichromatic quarter-wave plate (J. Fichou, Optique de Précision, Fresnes, France) was used. In order to get counterhelical writing beams, a half-wave plate at ω frequency was added in front of the bichromatic quarter-wave plate in order to achieve 90° rotation of the ω polarization without change on the 2ω polarization [Fig. 2(a)].

The photoinduced second-order susceptibility $\chi^{(2)}$ is probed using SH generation inside the sample. For this purpose, a RG630-Schott filter is periodically inserted in front of the sample, leaving only the fundamental beam incident on the sample.

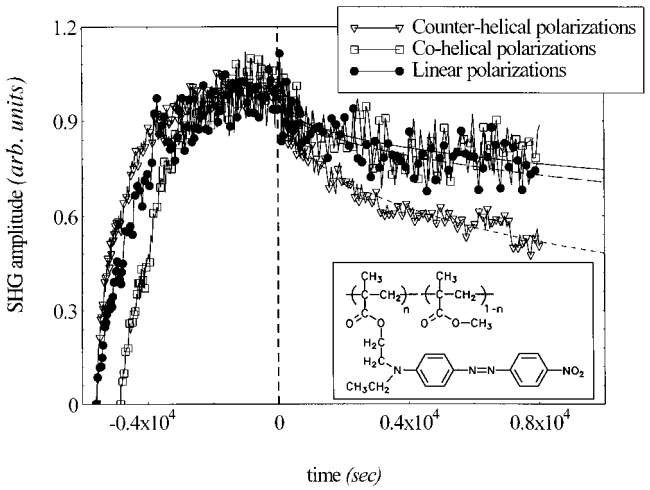

FIG. 3. Real-time growth and decay of the SH signal amplitude (proportional to $|\chi^{(2)}|$). Negative times correspond to the seeding preparation process. At time zero, the seeding process is stopped. Positive times correspond to $\chi^{(2)}$-susceptibility decay studies. Lifetime fitting was performed using stretched exponentials: $\chi^{(2)}\propto\exp(-t/\tau)^{\alpha}$, where τ is the time constant and α is the temporal dispersion. We get $\alpha\approx0.4$, $\tau_L\approx130$ s, $\tau_{C+}\approx230$ s, and $\tau_{C-}\approx20$ s, where the time constants correspond to linear, cohelical, and counterhelical writing beam polarizations, respectively. For helical writing beams, probing is achieved using a circularly polarized ω reading beam, analyzing the SH signal along the vertical direction (at 45° to X,Y, the quarter-wave plate neutral axes). For linearly polarized writing beams, the ω reading beam has the same polarization as the ω writing beam (vertical) and analysis of the second harmonic signal is also made along the same direction. In order to enable comparison of the photoinduced $\chi^{(2)}$ stability, all curves are normalized to the same maximum. Samples were a spin-coated 0.1-μm-thin films of the DR1-MMA 35/65 copolymer shown in inset ($n=0.35$). Its optical density was 0.3 at 532 nm. Peak intensity of the fundamental beams was about 1 GW/cm^2 and the 2ω writing beam was about a few MW/cm^2, corresponding to optimized intensities for efficient all-optical orientation.

B. Characterization of the photoinduced $\chi^{(2)}$

Samples were spin coated 0.1-μm-thin films of a polymethylmethacrylate (PMMA) polymer onto which Disperse Red 1 dye molecules were grafted with a 35% molar ratio (DR1-MMA 35/65 shown in inset of Fig. 3). The optical density at 532 nm was about 0.3.

Real-time growth and decay of the photoinduced second-order susceptibility $\chi^{(2)}$ are shown in Fig. 3 for each writing beam polarization combination. In all cases, we observe a gradual growth of the SH signal that saturates after comparable preparation time. All curves in Fig. 3 have been normalized to unity for display. In the case of linear writing beam polarizations, saturation is about one order of magnitude larger than in both cases of helical polarizations. This is a particular feature of in-plane poling efficiency, as discussed further in Sec. III D.

After poling, decay is multiexponential. Although photoinduced $\chi^{(2)}$ decays are comparable for linear and co-helical writing polarizations, a much faster decay of the photoinduced polar order is observed for counterhelical writing polarizations. Such a difference finds its origins in the dynamics of the poling process. Indeed, during all-optical

molecular orientation, orientation diffusion tends to restore initial isotropy. Moreover, depending on the polarization combinations of the writing beams, the cubic interference process gives rise to $\chi^{(2)}$ contributions with different amplitudes and relaxation times (see Appendix). In particular, in the case of counterhelical writing polarizations, the photoinduced $\chi^{(2)}$ results from a higher-order poling process (octupolar coupling) than in the case of linear and cohelical polarizations, thus leading to a reduced stability. In fact, linear or cohelical writing beams photoinduce a $\chi^{(2)}$ with both a long-living, dipolar and a short-living, octupolar contribution. However, in the latter two cases, as theoretically developed in Sec. 1 of the Appendix, the long-living dipolar term represents more than 80% of $\chi^{(2)}$. Unlike the theoretical dependence developed in the Appendix, a simple biexponential decay is not appropriate to fit the experimental $\chi^{(2)}$ temporal behavior. Indeed, the model developed in the Appendix is a simplified one: an appropriate model should go beyond the free rotator description, considering first that grafted molecules in a free volume are not simple free rotators but inhibited rotators owing to the polymer-dye interaction; second, it should include a distribution of diffusion constants accounting for molecules embedded with different free volumes [17]. As shown in Fig. 3, a stretched exponential model $\chi^{(2)} \propto \exp(-t/\tau)^{\alpha}$ is in good agreement with the experimental decay data, with τ representing the time constant and α representing the temporal dispersion. It also confirms the different features predicted in the simplified theory $\tau_L \approx \tau_{C+}$ and $\tau_{C-} \approx \tau_L/10$, with τ_L, τ_{C+}, and τ_{C-} the time constants associated with linear, cohelical, and counterhelical writing beam polarizations, respectively. So, we may conclude that the time constant in the multiexponential $\chi^{(2)}$ decay is relevant to the poling process (first-order dipolar or higher-order octupolar coupling).

C. Tensor analysis of the photoinduced $\chi^{(2)}$

Tensor analysis of the photoinduced $\chi^{(2)}$ was experimentally achieved by studying SH intensity generated along one given polarization direction as a function of the sample in-plane rotation angle δ. The ω reading beam was linearly polarized along the same direction [Fig. 2(b)] $\chi^{(2)}$ tensor polarization results are given in Figs. 4, 5, and 6, respectively, for the linear, cohelical, and counterhelical writing beam polarizations at ω and 2ω frequencies. Experimental data were recorded a few minutes after stopping the preparation process.

For linear writing beam polarizations, $\chi^{(2)}$ exhibits axial symmetry along the writing beam polarization direction. $\chi^{(2)}$ magnitude is strongly dependent on the phase difference $\Delta\Phi$ between the writing beams. The $\cos(3\delta)$ contribution of Eq. (A5a), which should yield an elongation of the $\chi^{(2)}$ lobes in Fig. 4, appears experimentally negligible, so that a $\cos(\delta)$ dependence is sufficient to account for the $\chi^{(2)}$ symmetries. The resulting tensor $\chi^{(2)}$ component corresponding to the in-plane map of the polar order is $\chi^{(2)}_{\Delta\Delta\Delta} \propto \cos(\Delta k \cdot z + \Delta\Phi)\cos(\delta)$. As a consequence, $\chi^{(2)}$ amplitude is sinusoidally modulated along the propagation direction with the period necessary for phase-matched second harmonic generation (right part of Fig. 4 [9]).

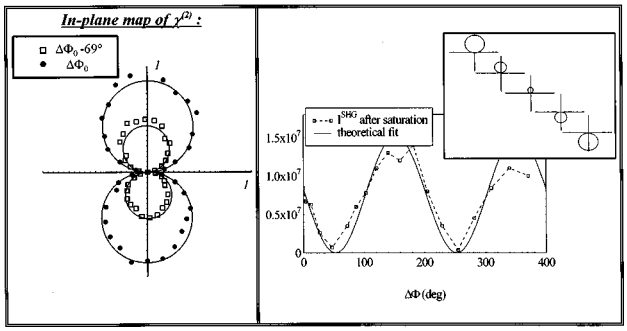

FIG. 4. $\chi^{(2)}$ symmetry for linear writing beam polarizations. The left part is the polar representation of the vertically polarized SH amplitude (defined as the square root of signal intensity $\alpha|\chi^{(2)}|$) as a function of the sample in-plane rotation. Two writing beam phase differences $\Delta\Phi$ obtained using two different tilt angles of the BK7 plate [see Fig. 2(a)] are displayed. As detailed in Fig. 2(b), the polar in-plane analysis of the photoinduced $\chi^{(2)}$ is performed using a linearly polarized reading beam at fundamental frequency. The SH signal generated along the same direction is analyzed as a function of the sample in-plane rotation. The solid line is the expected dipolar dependence deduced from Eq. (A5a): $|\chi^{(2)}_{\Delta\Delta\Delta}| \propto |\cos(\Delta k \cdot z + \Delta\Phi)\cos(\delta)|$. The right part of the figure shows the $|\chi^{(2)}|$ dependence with writing beams phase difference $\Delta\Phi$ [9]. The inset is a schematic polar representation of the amplitude-modulated $\chi^{(2)}$ over propagation.

For cohelical and counterhelical writing beam polarizations, $\chi^{(2)}$ magnitude is independent of the phase $\Delta\Phi$ between writing beams. In both cases, variation of the relative phase $\Delta\Phi$ yields in-plane rotation of the $\chi^{(2)}$ pattern by the same angle $\Delta\Phi$. Experimental data are in good agreement with the theoretical $\chi^{(2)}$ tensor components calculated in Sec. 2 of the Appendix. For cohelical writing beams, a nearly perfect dipolar C_1 symmetry is achieved. $\chi^{(2)}$ exhibits circu-

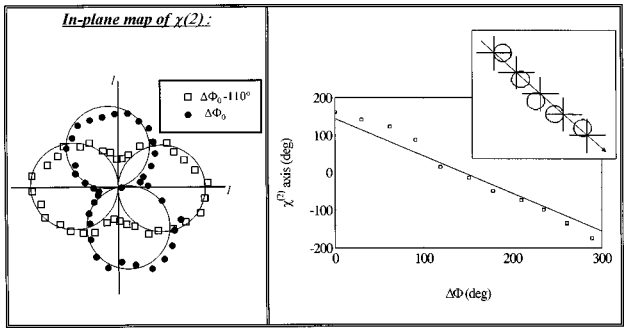

FIG. 5. $\chi^{(2)}$ symmetry for cohelical writing beam polarizations. The left part is the polar representation of the vertically polarized SH amplitude ($\alpha|\chi^{(2)}|$) as a function of the sample in-plane rotation. Two writing beam phase differences $\Delta\Phi$ obtained using two different tilt angles of the BK7 plate [see Fig. 2(a)] are displayed. As detailed in Fig. 2(b), the polar in-plane analysis of the photoinduced $\chi^{(2)}$ is performed using a linearly polarized reading beam at fundamental frequency. The SH signal generated along the same direction is analyzed as a function of the sample in-plane rotation. The solid line is the expected theoretical dependence of Eq. (A5b): $|\chi^{(2)}_{\Delta\Delta\Delta}| \propto |\cos(\Delta k \cdot z + \Delta\Phi + \delta)|$. The right part of the figure shows that the $\chi^{(2)}$ C_1 axis rotates like the writing beams phase difference $\Delta\Phi$. The inset is a schematic polar representation of the axis-modulated $\chi^{(2)}$ over propagation.

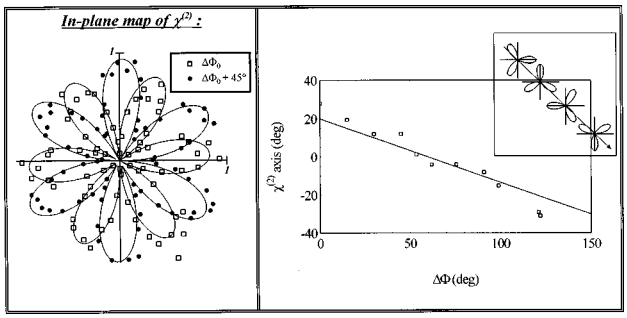

FIG. 6. $\chi^{(2)}$ symmetry for counterhelical writing beam polarizations. The left part is the polar representation of the vertically polarized SH amplitude ($\alpha|\chi^{(2)}|$) as a function of the sample in-plane rotation. Two writing beam phase differences $\Delta\Phi$ obtained using two different tilt angles of the BK7 plate [see Fig. 2(a)] are displayed. As detailed in Fig. 2(b), the polar in-plane analysis of the photoinduced $\chi^{(2)}$ is performed using a linearly polarized reading beam at fundamental frequency. The SH signal generalized along the same direction is analyzed as a function of the sample in-plane rotation. Solid and dotted lines are the expected theoretical dependence of Eq. (A5c): $|\chi^{(2)}_{\Delta\Delta\Delta}| \propto |\cos(\Delta k \cdot z + \Delta\Phi + 3\delta)|$. The right part of the figure shows that the $\chi^{(2)}$ C_3 axis rotates as $\Delta\Phi/3$. The inset is a schematic polar representation of the axis-modulated $\chi^{(2)}$ over propagation.

lar lobes as predicted by Eq. (A5b): $\chi^{(2)}_{\Delta\Delta\Delta} \propto \cos(\Delta k \cdot z + \Delta\Phi + \delta)$ (Fig. 5). The $\chi^{(2)}$ axis rotates exactly by the same angle as the writing beams' phase difference $\Delta\Phi$ (right part of Fig. 5). For counterhelical writing beams, a nearly perfect octupolar C_3 symmetry is achieved. The $\chi^{(2)}$ pattern exhibits petals as predicted by Eq. (A5c): $\chi^{(2)}_{\Delta\Delta\Delta} \propto \cos(\Delta k \cdot z + \Delta\Phi + 3\delta)$ (Fig. 6). The $\chi^{(2)}$ axis rotates as $\Delta\Phi/3$ (right part of Fig. 6). Worth noting is that in the latter case, the macroscopic $\chi^{(2)}$ exhibits octupolar symmetry although the nonlinear dye molecules exhibit one-dimensional symmetry. Worth noting also is that unlike the case of linear writing beam polarizations, helical writing beams yield only modulation of the $\chi^{(2)}$ axis, at the period necessary for phase-matched frequency doubling (insets in Figs. 5 and 6).

D. Photoinduced $\chi^{(2)}$ magnitude and phase-matching properties

All-optical poling with circular polarizations leads to richer tensor properties of $\chi^{(2)}$. As a consequence, for a circular reading beam polarization, the whole $\chi^{(2)}$ is phase matched for SH, which enables a larger conversion efficiency than in all-optical poling with linear polarizations, where only part of $\chi^{(2)}$ is phase matched (see Sec. 3a of the Appendix). Interestingly, in both cohelical and counterhelical writing beam polarizations, the generated SH signal is independent on the polarization direction when the fundamental reading beam polarization is linear (see Sec. 3b of the Appendix). Note, however, that in the case of counterhelical writing beam polarizations, the generated SH signal is perfectly circular whereas it is elliptical in the case of cohelical writing beam polarizations.

Additionally, the photoinduced SH signal results from different processes: excitation rate, molecular orientation efficiency and decay, and phase matching. In the case of cohelical and counterhelical writing beam polarizations, comparable SH intensities are achieved at saturation. In the case of linear writing beam polarizations, the saturated SH intensity is about 10 times larger. In the former case of helical writing polarizations, the fundamental reading polarization is circular and SH is analyzed along a given direction (at 45° to the quarter-wave plate neutral axes). The SH intensities developed in the Appendix are

$$I^{\mathrm{SH}}_{C+} = \frac{1}{2\times 140^2}\ \eta^2_{C+}\ \frac{\omega^2}{n^2c^2 10^{\mathrm{OD}}}\ I^2_\omega l^2$$

and

$$I^{\mathrm{SH}}_{C-} = \frac{1}{2\times 140^2}\ \eta^2_{C-}\ \frac{\omega^2}{n^2c^2 10^{\mathrm{OD}}}\ I^2_\omega l^2$$

for cohelical and counterhelical writing beam polarizations, respectively. OD is optical density and n is refractive index at 2ω, l is sample thickness, and I_ω is light intensity at ω. In the latter case of linear writing and reading beam polarizations, accounting for the sample thickness, which is much thinner than one coherence length, the optimum SH signal intensity is [9]. $I^{\mathrm{SH}}_L = (1/14^2)\,\eta^2_L(\omega^2/n^2c^2 10^{\mathrm{OD}}) I^2_\omega l^2$. So, experimental saturation values reveal that poling efficiencies η_{C+} and η_{C-} are comparable. However, a factor of 10 only between I^{SH}_{C+} and I^{SH}_L: $I^{\mathrm{SH}}_L / I^{\mathrm{SH}}_{C+} \approx 10$ indicates that the molecular orientation efficiency is much larger in the case of circular writing beam polarizations: $\eta_{C+} \approx \eta_{C-} \gg \eta_L$. The reason may be found in the dynamics of all-optical poling. Indeed, as can be inferred from SH construction in Fig. 3, net orientation of the molecules is not instantaneous, but the molecules must experience several excitation-relaxation cycles within the preparation time. Moreover, the excitation probability is the sum of three terms corresponding to one-photon absorption, two-photon absorption, and the interference between these two terms [10]. Only the last term bears polarity. The first two axial terms induce only birefringence. They align molecules in a plane perpendicular to the exciting beam polarization, these molecules being ''lost'' for immediate reexcitation along the same axis. In the case of circular writing beam polarizations, improved molecular orientation efficiency results from a much larger collection of molecules participating to the excitation-relaxation cycles, owing to in-plane molecular addressing, unlike linear addressing resulting from linear writing beam polarizations [18].

IV. CONCLUSION

Using appropriate combinations of the writing beam polarizations, dual-frequency interferences enable full control of the molecular polar order. It permits complete all-optical tailoring of the tensor properties of the photoinduced second-order susceptibility $\chi^{(2)}$, using conventional one-dimensional molecules. This aspect is of particular interest because one-dimensional molecules have been formerly tailored and optimized for stability, transparency, processability, and frequency conversion efficiency. A breakthrough is that, using light-matter interactions with circular beam polarizations, it becomes possible to achieve nearly perfect either dipolar or octupolar orders in a polymer consisting of one-dimensional molecules. Poling symmetry was not as clear

using linear polarizations with linear or octupolar molecules [12]. Worth noting also is that writing beam phase retardation $\Delta\Phi$ is coded into a $\chi^{(2)}$ pattern rotation by the same angle. This enables a polarization-independent second harmonic signal in the case of a linear fundamental reading beam. Dynamics of the photoinduced molecular orientation process show fairly good agreement with simplified theoretical predictions. Comparison of the saturated $\chi^{(2)}$ magnitude shows that circularly polarized writing beams improve all-optical poling efficiency. Experiments are in progress to apply these concepts to the preparation of polymer waveguides for efficient frequency doubling, in which an additional advantage may be taken from light confinement.

APPENDIX

1. Dynamics of the photoinduced polar order

Following the all-optical poling process, molecular orientation diffusion inside the polymer matrix tends to restore the initial isotropy of the material. In the case of free rotators, the temporal behavior of the photoinduced polar distribution $N_P(M)$ is driven by the rotational diffusion equation [19]:

$$\frac{dN_P}{dt} = -D\nabla^2 N_P, \tag{A1}$$

where D is the diffusion constant. Spherical harmonics $Y_1^m(\theta,\varphi)$ (where θ and φ are the Euler angles) are eigensolutions with eigenvalues $l(l+1)$ [20]. So, the relaxation time of each eigenterm is simply given by $\tau_l = 1/[l(l+1)D]$.

In order to separate contributions having different relaxation times, it is thus interesting to develop the polar distribution $N_p(M)$ as a linear combination of these spherical harmonics:

$$N_p = \sum_m [\alpha^{(1)} Y_1^m \exp(-2Dt) + \alpha^{(3)} Y_3^m \exp(-12Dt)]$$
$$= N_p^{(1)} \exp(-2Dt) + N_p^{(3)} \exp(-12Dt). \tag{A2}$$

Indeed, the distribution $N_p(M)$ being polar, only the odd-order terms l are present in the expansion. Additionally, the poling process resulting from a cubic interference process, the highest order l for the decomposition of $N_p(M)$ is $l=3$. After calculation we get the following terms for the first-order dipolar, and third-order octupolar terms $N_P^{(1)}$ and $N_P^{(3)}$:

$$N_p^{(1)} \propto \frac{1}{(1+\varepsilon_1^2)\sqrt{1+\varepsilon_2^2}} [\tfrac{1}{5} Y_1^0 (3+2\varepsilon_1\varepsilon_2-\varepsilon_1^2)\cos(\Delta k\cdot z+\Delta\Phi) - \tfrac{1}{5} Y_1^1 (2\varepsilon_1-\varepsilon_2+3\varepsilon_1^2\varepsilon_2)\sin(\Delta k\cdot z+\Delta\phi)], \tag{A3a}$$

$$N_p^{(3)} \propto \frac{1}{(1+\varepsilon_1^2)\sqrt{1+\varepsilon_2}} [\tfrac{1}{5} Y_3^0 (1-\varepsilon_1\varepsilon_2+\tfrac{1}{2}\varepsilon_1^2) + Y_3^2(-\varepsilon_1\varepsilon_2+\tfrac{1}{2}\varepsilon_1^2)]\cos(\Delta k\cdot z+\Delta\Phi) - [\tfrac{1}{5} Y_3^1(-\tfrac{3}{4}\varepsilon_1^2\varepsilon_2+2\varepsilon_1-\varepsilon_2)$$
$$-\tfrac{1}{4} Y_3^3(\varepsilon_1^2\varepsilon_2)]\sin(\Delta k\cdot z+\Delta\Phi), \tag{A3b}$$

with $Y_1^0=\cos\theta$, $Y_1^1=\sin\theta\sin\varphi$, $Y_3^0=5\cos^3\theta-3\cos\theta$, $Y_3^1=\sin\theta\sin\varphi(5\cos^2\theta-1)$, $Y_3^2=\sin^2\theta\cos\theta\cos2\varphi$, and $Y_3^3=\sin^3\theta\sin3\varphi$ [20].

Details of photoinduced polar distributions $N_P(M)$ corresponding to the different polarization combinations experimentally studied are given in Table I. Note that in the case of counterhelical writing beam polarizations ($\varepsilon_1=-\varepsilon_2=1$), the first-order dipolar term $N_P^{(1)}$ vanishes, leaving only the third-order octupolar one, $N_P(\varepsilon_1=-\varepsilon_2=1)\equiv N_P^{(3)}$.

As a consequence of molecular orientation following selective polar excitation, the photoinduced $\chi^{(2)}$ will also have two contributions with different relaxation times: $\chi^{(2)} = \chi_1^{(2)}\exp(-2Dt) + \chi_3^{(2)}\exp(-12Dt)$. Expressions of the first-order and third-order terms $\chi_1^{(2)}$ and $\chi_3^{(2)}$ are detailed in the following section for each writing beam polarization combi nation.

2. Tensor properties of the photoinduced $\chi^{(2)}$

a. Full tensor analysis

A general calculation of the SH signal as a function of one given ω reading beam polarization requires calculation of all $\chi^{(2)}$ tensor elements.

As stated in Sec. II, for an assembly of noninteracting molecules, macroscopic second-order susceptibility tensor elements $\chi_{XYZ}^{(2)}$ are related to the molecular hyperpolarizability β [16]: $\chi_{XYZ}^{(2)} = \eta\int N_P \beta_{XYZ}(\Omega)d\Omega/\varepsilon_0$, where β_{XYZ} is the projection of the molecular hyperpolarizability $\overline{\overline{\beta}}$ tensor along the given set of axes X,Y,Z: $\beta_{XYZ}(\Omega) = \Sigma_{x,y,z}(X\cdot x)(Y\cdot y)(Z\cdot z)\beta_{xyz}$, x,y,z referring to a set of unit vectors in the molecular reference frame. η is the efficiency of molecular orientation following polar selective excitation.

In the case of a one-dimensional molecule, the hyperpolarizability tensor $\overline{\overline{\beta}}$ has only one nonzero component along the molecular axis x: $\overline{\overline{\beta}} \equiv \beta(x\otimes x\otimes x)$. The expression for $\chi_{XYZ}^{(2)}$ simplifies to

$$\chi_{XYZ}^{(2)} = \eta\beta\int N_P (X\cdot x)(Y\cdot x)(Z\cdot x)d\Omega/\varepsilon_0. \tag{A4}$$

Tensor elements of the photoinduced susceptibility $\chi^{(2)}$ are given in Table II. In both linear and cohelical writing beam polarizations, where $\chi^{(2)}$ results from two contribu-

TABLE I. Summary of the photoinduced molecular polar distributions $N_p(M)$ induced with the different writing beam polarization configurations studied: case of linear polarizations (1), case of cohelical polarizations (2), and case of counterhelical polarizations (3). The first-order dipolar $N_p^{(1)}$ and third-order octupolar $N_p^{(3)}$ terms are given separately.

	$N_P = N_P^{(1)} + N_P^{(3)}$	
	$N_P^{(1)}$	$N_P^{(3)}$
(1) Linear polarizations $\varepsilon_1 = \varepsilon_2 = 0$	$\frac{3}{5} Y_1^0 \cos(\Delta k \cdot z + \Delta\Phi)$	$\frac{1}{5} Y_3^0 \cos(\Delta k \cdot z + \Delta\Phi)$
(2) Cohelical polarizations $\varepsilon_1 = \varepsilon_2 = 1$	$\left(\frac{1}{2\sqrt{2}}\right)[\frac{4}{5} Y_1^0 \cos(\Delta k \cdot z + \Delta\Phi) - \frac{4}{5} Y \vert \sin(\Delta k \cdot z + \Delta\Phi)]$	$\left(\frac{1}{2\sqrt{2}}\right)[(\frac{1}{10} Y_3^0 - \frac{1}{2} Y_3^2)\cos(\Delta k \cdot z + \Delta\Phi) - (\frac{1}{20} Y_3^1 - \frac{1}{4} Y_3^3)\sin(\Delta k \cdot z + \Delta\Phi)]$
(3) Counterhelical polarizations $\varepsilon_1 = -\varepsilon_2 = 1$	$\varnothing$	$\left(\frac{1}{2\sqrt{2}}\right)[(\frac{1}{2} Y_3^0 + \frac{3}{2} Y_3^2)\cos(\Delta k \cdot z + \Delta\Phi) - (\frac{3}{4} Y_3^1 + \frac{1}{4} Y_3^3)\sin(\Delta k \cdot z + \Delta\Phi)]$

tions with different relaxation times, the long living, first-order contribution is also given.

b. In-plane map of the photoinduced susceptibility

As stated in Eq. (4), for a given direction Δ in the plane of the sample, with Δ making an angle δ with axis X (Fig. 2), the photoinduced susceptibility $\chi^{(2)}_{\Delta\Delta\Delta}$ is written as $\chi^{(2)}_{\Delta\Delta\Delta} = \eta \int N_P \beta_{\Delta\Delta\Delta}(\Omega) d\Omega/\varepsilon_0$, with $\beta_{\Delta\Delta\Delta} = \beta(\Delta \cdot x)^3$ in the case of a one-dimensional molecule along the x axis and with η the orientation efficiency. Substitution of the polar distribution $N_p(M)$ for each writing beam polarization combination (Table I) leads to the following $\chi^{(2)}_{\Delta\Delta\Delta}$: (i) the linear writing beam polarization case

$$\chi^{(2)}_{\Delta\Delta\Delta} \propto \frac{1}{5}\, \eta_L \cos(\Delta k \cdot z + \Delta\Phi)\left[\frac{3}{5}\cos\delta \exp(-2Dt) + \frac{3\cos\delta + 5\cos 3\delta}{70}\exp(-12Dt)\right]; \qquad \text{(A5a)}$$

(ii) the cohelical writing beam polarization case

$$\chi^{(2)}_{\Delta\Delta\Delta} \propto \frac{1}{25\sqrt{2}}\, \eta_{C+} \cos(\Delta k \cdot z + \Delta\Phi + \delta)\left[2\exp(-2Dt) + \frac{1}{7}\exp(-12Dt)\right]; \qquad \text{(A5b)}$$

and (iii) the counterhelical writing beam polarization case

$$\chi^{(2)}_{\Delta\Delta\Delta} \propto \frac{1}{35\sqrt{2}}\, \eta_{C-} \cos(\Delta k \cdot z + \Delta\Phi + 3\delta)\exp(-12Dt), \qquad \text{(A5c)}$$

with η_1, η_{C+}, and η_{C-} the molecular reorientation efficiency in the case of linear, cohelical, and counterhelical writing beam polarizations, respectively.

In all cases, the photoinduced $\chi^{(2)}$ is sinusoidally modulated along the propagation direction with the period necessary for phase-matched second harmonic generation. However, unlike the case of linear writing beam polarizations resulting in a modulation of the photoinduced $\chi^{(2)}$ amplitude, in the case of helical writing beam polarizations, the only direction of the molecular order ($\chi^{(2)}$ axis) is modulated, with no amplitude variation. The incidence of such tensor properties on the phase-matched second harmonic signal is discussed in the following section.

3. Phase-matching properties

Evolution of the SH generated signal E^{SH} along one direction is driven by material losses and energy transfer between fundamental and second harmonic waves. The forward generated second harmonic field ($\mathbf{k}_{\mathrm{SH}} = \mathbf{k}_{2\omega}$) is solution of the following wave equation:

$$\frac{dE_{\mathrm{SH}}}{dt} = -\frac{\alpha}{2} E_{\mathrm{SH}} + \frac{i\omega}{nc}\frac{\mathbf{P}_{\mathrm{SH}} \cdot \varepsilon}{\varepsilon_0}\exp(i\Delta k \cdot z), \qquad \text{(A6)}$$

with $\Delta k = 2k_\omega - k_{2\omega}$ and where α and n represent the absorption coefficient and the refractive index of the material at 2ω frequency, respectively. P_{SH} is the second harmonic polarization generated by the photoinduced second-order susceptibility $\chi^{(2)}$ probed by a fundamental reading beam. ε is the unit polarization direction along which second harmonic generation is analyzed.

a. Case of an ω reading beam with circular polarization

Let us consider the case of an ω reading beam with circular polarization $\mathbf{E}_\omega = (1/\sqrt{2})\widetilde{E}_\omega(\mathbf{X} + j\mathbf{Y})$, with $\widetilde{E}_\omega$ the ω reading beam amplitude. Assuming a weak absorption at 2ω frequency, so that poling efficiency is homogeneous over propagation inside the sample, the SH polarization generated along the vector ε at 45° to the axes $\mathbf{X}$ and $\mathbf{Y}$ is

TABLE II. Theoretical photoinduced $\chi^{(2)}$ tensor components obtained for the different writing beam polarization configurations studied. For each component, the long-living dipolar first-order term of the photoinduced $\chi^{(2)}$ tensor is given separately.

	$\chi^{(2)}_{XXX}/\eta$		$\chi^{(2)}_{XYY}/\eta \equiv \chi^{(2)}_{YXY}/\eta$		$\chi^{(2)}_{YXX}/\eta \equiv \chi^{(2)}_{XXY}/\eta$		$\chi^{(2)}_{YYY}/\eta$	
	Global term	First-order term	Global term	First-order term	Global term	First-order term	Global term	First-order term
(1) Linear polarizations $\eta=\eta_L$	$\frac{1}{7}\cos \times(\Delta k\cdot z+\Delta\Phi)$	$\frac{3}{25}\cos \times(\Delta k\cdot z+\Delta\Phi)$	$\frac{1}{35}\cos \times(\Delta k\cdot z+\Delta\Phi)$	$\frac{1}{25}\cos \times(\Delta k\cdot z+\Delta\Phi)$	$\varnothing$	$\varnothing$	$\varnothing$	$\varnothing$
(2) Cohelical polarizations $\eta=\eta_{C+}$	$\frac{3}{35\sqrt{2}}\cos \times(\Delta k\cdot z+\Delta\Phi)$	$\frac{2}{25\sqrt{2}}\cos \times(\Delta k\cdot z+\Delta\Phi)$	$\frac{1}{35\sqrt{2}}\cos \times(\Delta k\cdot z+\Delta\Phi)$	$\frac{2}{75\sqrt{2}}\cos \times(\Delta k\cdot z+\Delta\Phi)$	$\frac{-1}{35\sqrt{2}}\sin \times(\Delta k\cdot z+\Delta\Phi)$	$\frac{-2}{75\sqrt{2}}\cos \times(\Delta k\cdot z+\Delta\Phi)$	$\frac{-3}{35\sqrt{2}}\sin \times(\Delta k\cdot z+\Delta\Phi)$	$\frac{-2}{25\sqrt{2}}\sin(\Delta k\cdot z+\Delta\Phi)$
(3) Counterhelical polarizations $\eta=\eta_{C-}$	$\frac{1}{35\sqrt{2}}\cos \times(\Delta k\cdot z+\Delta\Phi)$	$\varnothing$	$\frac{-1}{35\sqrt{2}}\cos \times(\Delta k\cdot z+\Delta\Phi)$	$\varnothing$	$\frac{-1}{35\sqrt{2}}\sin \times(\Delta k\cdot z+\Delta\Phi)$	$\varnothing$	$\frac{1}{35\sqrt{2}}\sin \times(\Delta k\cdot z+\Delta\Phi)$	$\varnothing$

$$\mathbf{P}_{\mathrm{SH}}\cdot\varepsilon=\frac{1}{4\sqrt{2}}\,\eta\varepsilon_0\tilde{E}_\omega^2[(\chi^{(2)}_{XXX}+\chi^{(2)}_{YYY}-\chi^{(2)}_{XYY}-\chi^{(2)}_{YXX}) +2j(\chi^{(2)}_{XYX}+\chi^{(2)}_{YYX})]\exp\left(-\frac{\alpha}{2}z\right). \tag{A7}$$

Tensor properties of $\chi^{(2)2}$ are highly dependent on the writing beam polarization combination. Resolution of the wave equation in the particular case of writing beams with linear polarizations has been developed previously [9]. In the following, we analyze more generally the incidence of the writing conditions on the SH signal.

As shown in Table II, for linear writing beam polarizations, the $\chi^{(2)}$ tensor is reduced to three components, and the SH polarization generated along ε can be written as $\mathbf{P}_{\mathrm{SH}}\cdot\varepsilon=(1/70\sqrt{2})\,\eta_L(2+j)\varepsilon_0\tilde{E}_\omega^2\cos(\Delta k\cdot z+\Delta\Phi)\exp[-(\alpha/2)z]$, where η_L stands for the molecular orientation efficiency of the writing process with linear polarizations. For a sample with thickness l larger than one coherence length, only half of $\mathbf{P}_{\mathrm{SH}}$ is phase matched and the SH intensity writes is written as

$$I_L^{\mathrm{SH}}=\left(\frac{\sqrt{5}}{140\sqrt{2}}\right)^2\frac{\omega^2\eta_L^2}{n^2c^2 10^{\mathrm{OD}}}\,I_\omega^2 l^2.$$

For writing beams with circular polarizations, the SH signal is circular. SH polarization generated along ε is

$$\mathbf{P}_{\mathrm{SH}}\cdot\varepsilon=\frac{1}{70\sqrt{2}}\,\varepsilon_0\tilde{E}_\omega^2\eta_{C+/C-}\,\exp\left[-j\left(\Delta k\cdot z+\Delta\Phi-\frac{\pi}{4}\right)\right]\times\exp\left(-\frac{\alpha}{2}z\right)$$

for cohelical $(C+)$ and counterhelical $(C-)$ writing beam polarizations, respectively. In both cases, the full term leads to phase-matched second harmonic generation so that SH intensity is written as

$$I_{C+/C-}^{\mathrm{SH}}=\left(\frac{1}{140\sqrt{2}}\right)^2\frac{\omega^2\eta_{C+/C-}^2}{\eta^2c^2 10^{\mathrm{OD}}}\,I_\omega^2 l^2$$

for cohelical and counterhelical polarizations, respectively. Consequently, assuming comparable all-optical poling efficiencies, writing with helical polarizations is all the more interesting since it enables one to take full advantage of the tensor properties of $\chi^{(2)}$.

b. Case of an ω reading beam with linear polarization

If we consider now the case of an ω reading beam with a linear polarization in a given direction making an angle ρ with axis X, $E_\omega=(\cos\rho\mathbf{X}+\sin\rho\mathbf{Y})\tilde{E}_\omega$, with $\tilde{E}_\omega$ the ω reading beam amplitude. Assuming again a weak absorption at 2ω frequency, so that poling efficiency is homogeneous over propagation inside the sample, the SH polarization is

$$\mathbf{P}_{\mathrm{SH}}^{C+} \propto \exp[-(\alpha/2)z]\{[(1+2\cos^2\rho)\cos(\Delta k\cdot z+\Delta\Phi)-\sin(2\rho)\sin(\Delta k\cdot z+\Delta\Phi)]\mathbf{X}-[(1+2\sin^2\rho)\sin(\Delta k\cdot z+\Delta\Phi) - \sin(2\rho)\cos(\Delta k\cdot z+\Delta\Phi)]\mathbf{Y}\}, \tag{A8a}$$

$$\mathbf{P}_{\mathrm{SH}}^{C-} \propto \exp[-(\alpha/2)z]\{[\cos(2\rho)\cos(\Delta k\cdot z+\Delta\Phi)-\sin(2\rho)\sin(\Delta k\cdot z+\Delta\Phi)]\mathbf{X} - [\cos(2\rho)\sin(\Delta k\cdot z+\Delta\Phi)+\sin(2\rho)\cos(\Delta k\cdot z+\Delta\Phi)]\mathbf{Y}\} \tag{A8b}$$

in the case of cohelical $(C+)$ and counterhelical $(C-)$ writing beam polarizations, respectively.

After resolution of the propagation equation, considering a sample thickness l larger than one coherence length, the generated SH amplitude coming from the phase-matched terms is

$$A_{\mathrm{SH}}^{C+} \propto \{[(1+2\cos^2\rho)+j\ \sin(2\rho)]\mathbf{X}-[(1+2\sin^2\rho)j-\sin(2\rho)]\mathbf{Y}\}l\ \exp[-(\alpha/2)l] \tag{A9a}$$

$$A_{\mathrm{SH}}^{C-} \propto \{[\cos 2\rho - j\ \sin(2\rho)]\mathbf{X}-[j\ \cos 2\rho+\sin(2\rho)]\mathbf{Y}\}l\ \exp[-(\alpha/2)l]. \tag{A9b}$$

It implies that, in both cases of cohelical or counterhelical writing beam polarizations, the photoinduced $\chi^{(2)}$ gives rise to a total SH intensity $I_{\mathrm{SH}}=|\mathbf{A}_{\mathrm{SH}}\cdot\mathbf{X}|^2+|\mathbf{A}_{\mathrm{SH}}\cdot\mathbf{Y}|^2$ independent on the ω reading beam polarization direction ρ. Note, however, that in the case of counterhelical writing beams polarizations, the generated SH signal is perfectly circular whereas it is elliptical in the case of cohelical writing beam polarizations.

[1] P. Brumer and M. Shapiro, Annu. Rev. Phys. Chem. **43**, 257 (1992).

[2] G. Kurizki, M. Shapiro, and P. Brumer, Phys. Rev. B **39**, 3435 (1989).

[3] U. Österberg and W. Margulis, Opt. Lett. **11**, 516 (1986).

[4] R. H. Stolen and H. W. K. Tom, Opt. Lett. **12**, 585 (1987).

[5] T. J. Driscoll and N. M. Lawandy, J. Opt. Soc. Am. B **11**, 355 (1994).

[6] T. J. Driscoll, R. L. MacDonald, and N. M. Lawandy, Phys. Rev. A **48**, 3278 (1993).

[7] V. Dominic and J. Feinberg, Phys. Rev. Lett. **71**, 3446 (1993).

[8] F. Charra, F. Devaux, J.-M. Nunzi, and P. Raimond, Phys. Rev. Lett. **68**, 2440 (1992).

[9] C. Fiorini, F. Charra, J. M. Nunzi, and P. Raimond, Nonlinear Opt. **9**, 339 (1995).

[10] C. Fiorini, F. Charra, J. M. Nunzi, and P. Raimond, J. Opt. Soc. Am. B **108**, 1984 (1997).

[11] J. M. Nunzi, F. Charra, C. Fiorini, and J. Zyss, Chem. Phys. Lett. **219**, 349 (1994).

[12] C. Fiorini, F. Charra, J. M. Nunzi, I. D. W. Samuel, and J. Zyss, Opt. Lett. **20**, 2469 (1995).

[13] N. B. Baranova and B. Ya. Zeldovich, JETP Lett. **45**, 717 (1987)].

[14] C. Fiorini, F. Charra, and J. M. Nunzi, J. Opt. Soc. Am. B **11**, 2347 (1994).

[15] C. Fiorini, J. M. Nunzi, F. Charra, I. D. W. Samuel, and J. Zyss, J. Nonlin. Opt. Phys. Mat. **5**, 653 (1996).

[16] K. D. Singer, M. G. Kuzyk, and J. E. Sohn, J. Opt. Soc. Am. B **4**, 968 (1987).

[17] J. G. Victor and J. M. Torkelson, Macromolecules **20**, 2242 (1987).

[18] X. L. Jiang, L. Li, J. Kumar, and S. K. Kumar, Appl. Phys. Lett. **69**, 3629 (1996).

[19] H. J. Eichler, P. Günter, and D. W. Pohl, *Laser Induced Dynamic Gratings*, Springer Series in Optical Science Vol. 50 (Springer-Verlag, Berlin, 1986), p. 52.

[20] J. D. Jackson, *Classical Electrodynamics*, 2nd ed. (Wiley, New York, 1975), Chap. 3, p. 98.